

GAS-GRAIN MODELS FOR INTERSTELLAR ANION CHEMISTRY

M. A. CORDINER¹ AND S. B. CHARNLEY

Astrochemistry Laboratory and the Goddard Center for Astrobiology, Mailstop 691, NASA Goddard Space Flight Center, 8800
Greenbelt Road, Greenbelt, MD 20770, USA

Draft version June 11, 2018

ABSTRACT

Long-chain hydrocarbon anions C_nH^- ($n = 4, 6, 8$) have recently been found to be abundant in a variety of interstellar clouds. In order to explain their large abundances in the denser (prestellar/protostellar) environments, new chemical models are constructed that include gas-grain interactions. Models including accretion of gas-phase species onto dust grains and cosmic-ray-induced desorption of atoms are able to reproduce the observed anion-to-neutral ratios, as well as the absolute abundances of anionic and neutral carbon chains, with a reasonable degree of accuracy. Due to their destructive effects, the depletion of oxygen atoms onto dust results in substantially greater polyne and anion abundances in high-density gas (with $n_{H_2} \gtrsim 10^5 \text{ cm}^{-3}$). The large abundances of carbon-chain-bearing species observed in the envelopes of protostars such as L1527 can thus be explained without the need for warm carbon-chain chemistry. The C_6H^- anion-to-neutral ratio is found to be most sensitive to the atomic O and H abundances and the electron density. Therefore, as a core evolves, falling atomic abundances and rising electron densities are found to result in increasing anion-to-neutral ratios. Inclusion of cosmic-ray desorption of atoms in high-density models delays freeze-out, which results in a more temporally-stable anion-to-neutral ratio, in better agreement with observations. Our models include reactions between oxygen atoms and carbon-chain anions to produce carbon-chain-oxide species C_6O , C_7O , HC_6O and HC_7O , the abundances of which depend on the assumed branching ratios for associative electron detachment.

Subject headings: astrochemistry – ISM: abundances – ISM: clouds – ISM: molecules

1. INTRODUCTION

Hydrocarbon anions have been shown to be an important part of the molecular inventory of the Galaxy by their recent discoveries in the quiescent molecular clouds TMC-1 (McCarthy et al. 2006) and Lupus-1A (Sakai et al. 2010), the prestellar cores L1544 and L1512 and the envelopes of the low-mass protostars L1527, L1251A and L1521F (Sakai et al. 2007; Gupta et al. 2009; Cordiner et al. 2011). Previous chemical models have been able to reproduce with reasonable accuracy the observed abundances of C_6H^- and C_8H^- in TMC-1 and IRC+10216 (*e.g.* Millar et al. 2007; Remijan et al. 2007; Cordiner et al. 2008; Walsh et al. 2009), but not so well in the denser environment of L1527 (Harada & Herbst 2008). The abundances of CN^- and C_3N^- observed in IRC+10216 (Thaddeus et al. 2008; Agúndez et al. 2010) closely match the predictions made by the chemical model of Cordiner & Millar (2009). These studies show that the basic gas-phase chemical processes involving molecular anions are fairly well understood. So far, however, interactions between negatively-charged gas-phase species and dust grain surfaces have been largely neglected in chemical models for anions. Flower et al. (2007) modelled the C_6H^- to C_6H abundance ratio ($[C_6H^-]/[C_6H]$) in ‘typical’ dark-cloud gas (with density 10^4 cm^{-3}), using a chemical model accounting for the detailed calculation of charge balance, including gas, dust grain and PAH charge exchange, but did not consider the effects of depletion/freeze-out of molecules

onto the grains. Gas-grain interactions are theorized to be of fundamental importance for the abundances of gas-phase molecules in dense interstellar clouds (*e.g.* Brown & Charnley 1990), and Cordiner et al. (2011) proposed that oxygen freeze-out could help to explain the large abundances of carbon-chain-bearing species and anions observed in low-mass protostellar envelopes and prestellar cores with densities $n_{H_2} \sim 10^5 - 10^6 \text{ cm}^{-3}$.

The total abundance of molecular anions is believed to be an important factor affecting the ionization balance of the interstellar medium (ISM) (*e.g.* Lepp & Dalgarno 1988; Flower et al. 2007; Wakelam & Herbst 2008). Anion abundances are theorized to be sensitive to electron attachment and photodetachment rates, and may therefore provide a useful tool for the determination of electron densities and cosmic ray/photo-ionization rates in astrophysical environments (Millar et al. 2007; Flower et al. 2007). As shall become apparent from the present study, the interstellar C_6H^- anion-to-neutral ratio can also be a tracer of the abundances of gas-phase atomic hydrogen, oxygen and carbon, due to the rapid reactions between hydrocarbon anions and these species.

This article presents new chemical models for interstellar carbon chains and their anions, with the aim of understanding the more recent C_6H^- detections in relatively dense prestellar cores and cold protostellar envelopes. The inclusion of gas-grain interactions at varying levels of complexity permits analysis of the importance of these processes for anion chemistry, particularly at higher densities. We also discuss the possibility that reactions between hydrocarbon anions and oxygen atoms can produce detectable abundances of the carbon chain oxides C_nO and HC_nO ($n = 6, 7$) and the smaller hydro-

martin.cordiner@nasa.gov

¹ Institute for Astrophysics and Computational Sciences, The Catholic University of America, Washington, DC 20064, USA

carbon anion C_2H^- ; these species are yet to be detected in space.

2. CHEMICAL MODELLING

The chemical models presented here utilize the (dipole-enhanced) RATE06 network (Woodall et al. 2007), augmented with the anion chemistry of Walsh et al. (2009), and extended further to include C_3H^- and C_2H^- . Anions in the model are formed by radiative electron attachment, with rates taken from the calculations by Herbst & Osamura (2008). Anions are destroyed in reactions with H, C, N and O atoms and in mutual-neutralisation reactions with the most abundant cations (including C^+ , H^+ , H_3^+ and HCO^+). Product branching ratios for anion-neutral reactions are taken from Eichelberger et al. (2007), with additional data from V. Bierbaum (private communication, 2010). For reactions involving C_3H^- , the average was taken of the published rate coefficients for C_2H^- and C_4H^- . In addition to the C_3O molecule already present in the RATE06 network, we have added the longer carbon-chain oxides C_nO , HC_nO (for $n = 6$ and 7), as well as their protonated forms ($(\text{H})\text{C}_n\text{OH}^+$) and anions ($(\text{H})\text{C}_n\text{O}^-$) (see Section 5 for details). PAHs have not been included in our models due to a lack of evidence concerning their abundances in dark molecular clouds (Peeters 2011).

The abundances of 454 gas-phase species are calculated as a function of time, linked by 5132 binary reactions. Models begin at time $t = 0$ with neutral atomic abundances given in Table 1. The abundances of heavier metals (Na, Mg, Fe, P etc.) are set to zero, consistent with their non-detection in the ISM (Turner 1991). The cosmic ray ionisation rate is set at $1.3 \times 10^{-17} \text{ s}^{-1}$ and the visual extinction (A_V) is set to 10 mag. Hydrogen is predominantly molecular and models are run at densities $n_{\text{H}_2} = 10^4$, 10^5 and 10^6 cm^{-3} . These span the range of interstellar cloud densities where anions have so far been observed, from quiescent, dense molecular clouds (e.g. TMC-1, with $n_{\text{H}_2} = 10^4 \text{ cm}^{-3}$), to prestellar cores (e.g. L1512, with $n_{\text{H}_2} = 10^5 \text{ cm}^{-3}$) and protostellar envelopes (e.g. L1527, with $n_{\text{H}_2} = 10^6 \text{ cm}^{-3}$). The kinetic temperature is fixed at 10 K. These simplified models are useful for analysing basic astrochemical processes, and we do not consider the impact on the chemistry of protostellar heating, nor dynamical effects such as infall or outflows that may be present in some of the sources. Throughout this article, fractional abundances are given with respect to the total H_2 number density (n_{H_2}).

2.1. Model I: No accretion

Our first model considers only gas-phase chemistry and neglects the gas-grain interaction apart from the formation of H_2 on dust grains, which is assumed to occur at a rate $4.7 \times 10^{-18} n_{\text{H}}(n_{\text{H}} + 2n_{\text{H}_2})$. This modelling approach is the same as that used by Harada & Herbst (2008) for L1527 and Walsh et al. (2009) for TMC-1 and is therefore useful as a benchmark for comparison with those models. For details of the modelling procedure see Woodall et al. (2007) and Walsh et al. (2009).

2.2. Model II: Accretion without desorption

This model builds on Model I with the inclusion of gas-grain interactions. These are treated using the approach

of Charnley (1997), whereby gas-phase species (except for the highly volatile H^+ , H_2 , He and H_3^+) that collide with dust grains have a certain probability of sticking to the surface. We model a dust grain population composed of three distinct charge states: G^0 (neutral), G^+ (single positive charge) and G^- (single negative charge). Due to electrostatic repulsion, anions are assumed not to stick to negatively-charged grains. Anions undergo mutual-neutralisation upon collision with positively-charged grains, resulting in transfer of an electron from the anion (X^-) to the grain, and returning the neutral species (X) to the gas. Positive ions (X^+) undergo mutual-neutralisation in collisions with negatively-charged grains, again returning the neutral species (X) to the gas. The dust grain charges are calculated as a function of time using the formulation of Umebayashi & Nakano (1990) for a uniform-size grain population, with the addition of the anion-grain processes mentioned above. The parameters used are: dust grain radius = 10^{-5} cm , dust grain abundance = 2.0×10^{-12} , electron sticking-coefficient = 0.6, gas sticking-coefficient = 1, temperature $T = T_{\text{dust}} = T_{\text{gas}}$. The charge balance for this chemical plasma is

$$\sum_{\text{X}^-} n(\text{X}^-) + n(\text{G}^-) + n_e = \sum_{\text{X}^+} n(\text{X}^+) + n(\text{G}^+) \quad (1)$$

where the sums are over the number densities of all anions (X^-) and cations (X^+) in the model.

Due to the rapidity of collisions of electrons with the grains (as compared to cations with grains), the majority of the dust attains a negative charge soon after the start of the model, resulting in an approximately steady fraction of $\sim 90\%$ of the total number of grains as G^- during the chemically-relevant timescales. At a density of 10^6 cm^{-3} , gas-grain collisions result in near-complete depletion of the gas after $\sim 10^5 \text{ yr}$ (see Figure 3, middle panel).

2.3. Model III: Accretion with desorption of atoms

Gas-phase species deposited on the dust grains build up over time to form an icy mantle (see for example Öberg et al. 2011). Energetic processes are theorized to result in the liberation of mantle species back into the gas phase (Leger et al. 1985). Thermal desorption is very slow at dust temperatures of 10 K, and we assume that photo-desorption may be neglected in the dark clouds we are considering. However, heating of the dust grains by cosmic ray impact results in significantly elevated temperatures for short time periods, sufficient for volatile species to be quite rapidly desorbed (Hasegawa & Herbst 1993). Earlier models have proposed that atoms may either stick inefficiently on dust grains, or are selectively desorbed with respect to molecules (Hasegawa & Herbst 1993; Charnley et al. 2001; Flower et al. 2005). In our final model, we utilize the rate coefficients for cosmic-ray-induced desorption of C, N, O and S atoms calculated by Hasegawa & Herbst (1993). For simplicity, and due to their expected higher binding energies, desorption of molecular species is not considered.

3. RESULTS

For each of the three models, fractional abundances of the carbon-chain-bearing species HC_3N , C_4H , C_6H

TABLE 1
INITIAL FRACTIONAL
ABUNDANCES

Species	Abundance ^a
H	1.0×10^{-3}
He	2.8×10^{-1}
C	1.2×10^{-4}
N	4.0×10^{-5}
O	3.2×10^{-4}
S	2.0×10^{-8}

^a Relative to n_{H_2} .

and anions C_4H^- and C_6H^- are plotted as a function of time in Figures 1-3 at densities $n_{\text{H}_2} = 10^4$, 10^5 and 10^6 cm^{-3} , respectively. Horizontal broken lines show the observed fractional abundances of each species: for $n_{\text{H}_2} = 10^4 \text{ cm}^{-3}$, TMC-1 data are shown and for $n_{\text{H}_2} = 10^5 \text{ cm}^{-3}$, L1512 data are shown. For $n_{\text{H}_2} = 10^6 \text{ cm}^{-3}$, observed abundances are plotted for three sources: the pre-stellar core L1544 (dashed lines), the very low-luminosity, young protostar L1521F (dotted lines), and the Class 0/I protostar L1527 (dot-dashed lines). We briefly examine the results obtained for each density regime.

3.1. $n_{\text{H}_2} = 10^4 \text{ cm}^{-3}$ – Quiescent molecular cloud

For $n_{\text{H}_2} = 10^4 \text{ cm}^{-3}$ (Figure 1), Models I-III achieve a reasonable match with observations of the quiescent molecular cloud TMC-1 (within about an order of magnitude) at times around 10^5 yr , consistent with previous models for this source (*e.g.* Herbst & Leung 1989; Walsh et al. 2009). At times later than this, the HC_3N and C_4H abundances fall well below their respective observed values.

Interstellar polyynes (C_nH) and cyanopolyynes (HC_nN) chemistry was discussed by Walsh et al. (2009); polyynes are radical species and react rapidly with oxygen atoms whereas the closed-shell cyanopolyynes do not. Thus, in Model II the freezing-out of atomic oxygen onto dust grains eliminates one of the main polyynene destruction channels which significantly extends their lifetime in the gas. HC_3N , on the other hand, is primarily destroyed by reaction with C^+ and continues to fall in a similar manner between 10^5 and 10^6 yr independently of whether O-atoms are accreting out (see Figure 1, upper and middle panels). The cosmic-ray-desorption of O-atoms that occurs in Model III (Figure 1, lower panel) results in similar abundances to Model I because at this relatively low density the gas accretion rate is sufficiently low that it is counteracted by cosmic-ray desorption, which keeps the majority of material off the dust and in the gas-phase.

At a time of 10^5 yr , the modelled C_6H^- anion-to-neutral ratio $[\text{C}_6\text{H}^-]/[\text{C}_6\text{H}]$ is equal to 2.3% in all three models with $n_{\text{H}_2} = 10^4 \text{ cm}^{-3}$ and is thus apparently quite insensitive to gas-grain interactions at this time. The anion-to-neutral ratio rises at later times, predominantly as a result of rising electron densities and falling atomic H, C and O abundances (see Section 6). Comparison of the modelled anion-to-neutral ratio with the observed values given in Table 2 shows good agreement with the quiescent clouds TMC-1 and Lupus 1A.

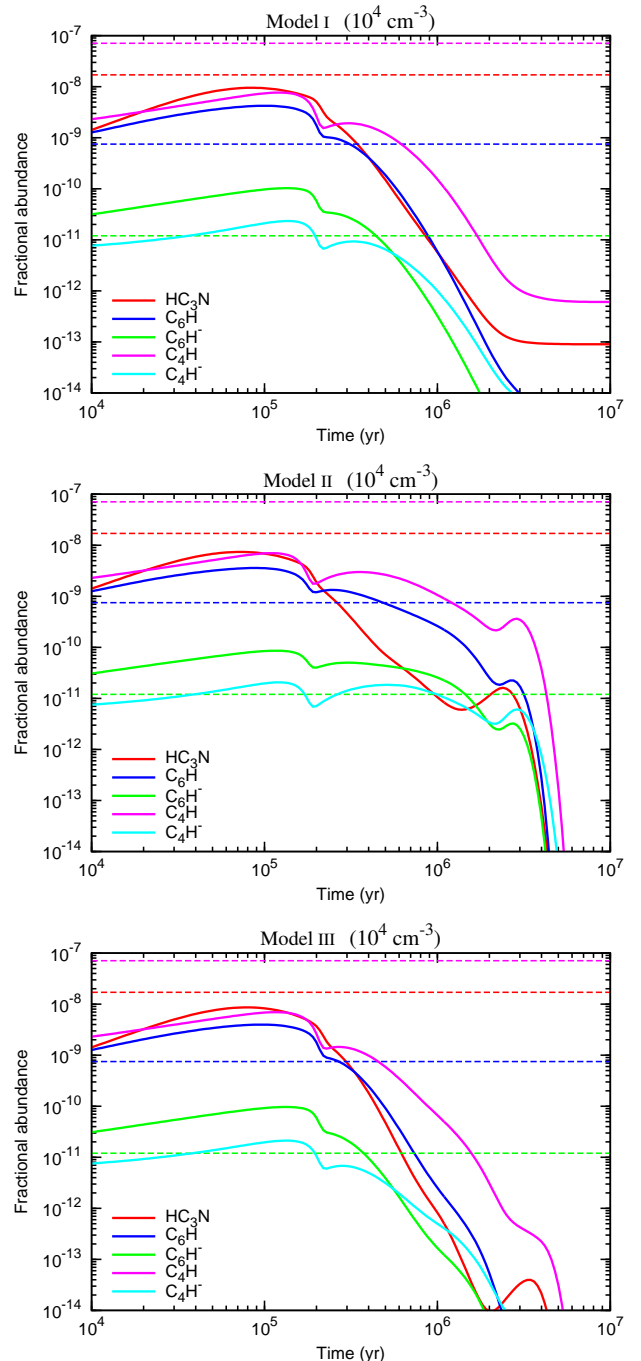


FIG. 1.— Carbon chain and anion fractional abundances as a function of time for $n_{\text{H}_2} = 10^4 \text{ cm}^{-3}$. Results of Model I (no accretion) are shown in the top panel, Model II (accretion with no desorption) in the middle panel and Model III (accretion + CR-desorption) in the bottom panel. TMC-1 observed abundances are shown with dashed lines (data from Suzuki et al. 1992; Brünken et al. 2007; Agúndez et al. 2008, with $N(\text{H}_2) = 1.0 \times 10^{22} \text{ cm}^{-2}$ from Cernicharo & Guélin 1987).

3.2. $n_{\text{H}_2} = 10^5 \text{ cm}^{-3}$ – Prestellar core

At $n_{\text{H}_2} = 10^5 \text{ cm}^{-3}$ (Figure 2), a reasonable agreement is obtained with observations of the prestellar core L1512 at times around $(6-8) \times 10^4 \text{ yr}$. The polyynes and anions in Models I and III (top and bottom panels) show a good fit to observations at this time (within a factor of a few), but HC_3N is significantly over-predicted. On the other

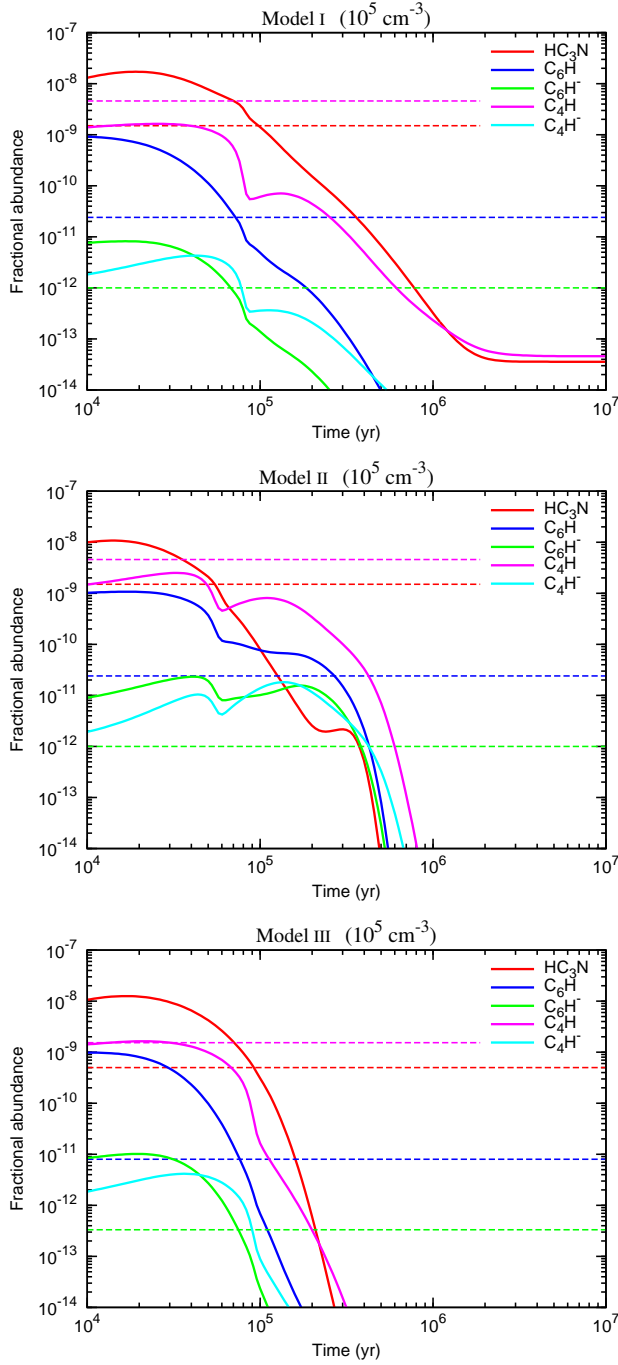


FIG. 2.— As Figure 1 but for $n_{\text{H}_2} = 10^5 \text{ cm}^{-3}$. L1512 observed abundances are shown with dashed lines (data from Cordiner et al. 2011, with $N(\text{H}_2) = 2.0 \times 10^{22} \text{ cm}^{-2}$ from Kirk et al. 2005).

hand, in Model II (with freeze-out and no desorption), HC_3N matches observations at about 6×10^4 yr whereas C_6H and C_6H^- are over-predicted by about an order of magnitude; the abundances of the latter are greater as a result of O-atom freeze-out.

The best fit to the observed C_6H^- anion-to-neutral ratios in the sources with $n_{\text{H}_2} = 10^5 \text{ cm}^{-3}$ (L1512 and L1251A; see Table 2) is also obtained in Models I and III, at around 7×10^4 yr, at which time $[\text{C}_6\text{H}^-]/[\text{C}_6\text{H}] = 3.1\%$ and 3.5% respectively. The freeze-out model with no desorption (Model II), significantly over-predicts the anion-

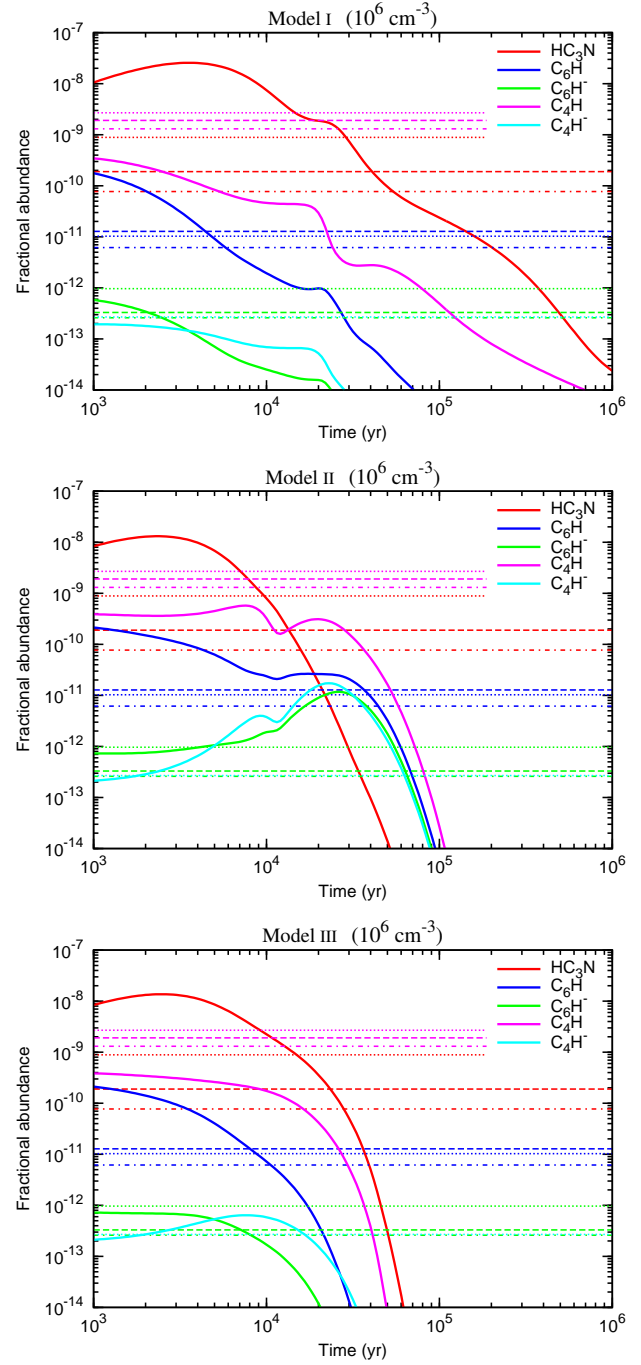


FIG. 3.— As Figure 1 but for $n_{\text{H}_2} = 10^6 \text{ cm}^{-3}$. L1544 abundances are shown with dashed lines (data from Suzuki et al. 1992 and Gupta et al. 2009, with $N(\text{H}_2) = 9.4 \times 10^{22} \text{ cm}^{-2}$ from Crapsi et al. 2005). L1521F abundances are shown with dot-dashed lines (Gupta et al. 2009, and our own unpublished Onsala 3 mm HC_3N data – for details of the Onsala observations see Buckle et al. 2006. We used $N(\text{H}_2) = 1.4 \times 10^{23} \text{ cm}^{-2}$ from Crapsi et al. 2005). L1527 abundances plotted with dotted lines (Jørgensen et al. 2004; Sakai et al. 2007; Agúndez et al. 2008, with $N(\text{H}_2) = 9.4 \times 10^{22} \text{ cm}^{-2}$ from Jørgensen et al. 2002). The L1527 C_4H^- abundance (cyan dotted line) is 2.7×10^{-13} and lies just above the L1521F C_6H^- abundance (green dot-dashed line).

TABLE 2
OBSERVED ANION-TO-NEUTRAL RATIOS, DENSITIES AND CO
DEPLETION FACTORS IN DENSE CLOUD CORES

Source	$[\text{C}_6\text{H}^-]/[\text{C}_6\text{H}]$	n_{H_2} (cm^{-3})	$\delta(\text{CO})$	Refs.
TMC-1	$1.6 \pm 0.3\%$	$\sim 10^4$	1.2 ^a	1, 2, 3
Lupus-1A	$2.1 \pm 0.6\%$	4
L1512	$4.2 \pm 1.4\%$	$\sim 10^5$	3.9 ^b	5, 6, 7
L1251A	$3.6 \pm 1.3\%$	$\sim 10^5$...	5, 8
L1544	$2.5 \pm 0.8\%$	$\sim 10^6$	7-14	9, 10, 11
L1521F	$4.0 \pm 1.0\%$	$\sim 10^6$	12-15	9, 10, 12
L1527	$9.3 \pm 2.9\%$	$\sim 10^6$	2.4 ^a	13, 14

REFERENCES. — (1) – Brünken et al. (2007); (2) – Hirahara et al. (1992); (3) – Ohishi et al. (1992); (4) – Sakai et al. (2010); (5) – Cordiner et al. (2011); (6) – Kirk et al. (2005); (7) – Lee et al. (2003); (8) – Lee et al. (2010); (9) – Gupta et al. (2009); (10) – Crapsi et al. (2005); (11) – Caselli et al. (2002); (12) – Crapsi et al. (2004); (13) – Sakai et al. (2007); (14) – Jørgensen et al. (2004).

^a Calculated from CO observations assuming an undepleted abundance of $9.5 \times 10^{-5} n_{\text{H}_2}$.

^b The Lee et al. (2003) CO depletion factor in L1512 has been scaled by 0.35 to account for the greater undepleted CO abundance of $2.7 \times 10^{-4} n_{\text{H}_2}$ used in that study.

to-neutral ratio at this time ($[\text{C}_6\text{H}^-]/[\text{C}_6\text{H}] = 8\%$) due to the larger radiative electron attachment rate that results from the greater electron density that occurs during freeze-out (see Section 6).

3.3. $n_{\text{H}_2} = 10^6 \text{ cm}^{-3}$ – Dense prestellar core / cold protostellar envelope

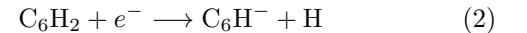
Gas-grain interactions are more rapid at higher densities, so at $n_{\text{H}_2} = 10^6 \text{ cm}^{-3}$ the effects of accretion on the modelled abundances are quite significant, as can be seen by comparison of the three panels in Figure 3. Gas-phase chemistry also proceeds more rapidly at high densities: without accretion (top panel), the conversion of C into CO (through the reaction of C and O_2), and the presence of abundant gas-phase O-atoms that react with and destroy the polyynes results in steadily diminishing carbon chain abundances over time. Accordingly, the Model I abundances fail to match observations of L1544, L1521F or L1527 at any time.

The inclusion of gas-grain interactions results in substantially greater carbon chain abundances for $t \gtrsim 1000$ yr in Model II compared with Model I. Indeed, Model II shows a good fit (within an order of magnitude), to the observed abundances in L1544, L1521F and L1527 at $t \sim 10^4$ yr. The only species that does not fit well with observations is C_4H^- , which has been over-predicted by at least an order of magnitude in all previous chemical models for this species (Millar et al. 2007; Flower et al. 2007; Harada & Herbst 2008; Walsh et al. 2009; Cordiner & Millar 2009). The most likely explanation for this discrepancy is a problem with the theoretical radiative electron attachment rate for C_4H , which was calculated using a relatively simplistic phase-space approach (for further discussion see Herbst & Osamura 2008).

The inclusion of cosmic-ray-induced desorption (Model III) diminishes the polyyne and anion abundances somewhat compared with Model II, primarily due to the increased gas-phase abundance of destructive O-atoms. The peak that occurs in the polyyne abundances in Model II towards the time of freeze-out is eliminated, but

a good fit to observations is still achieved at $\sim 10^4$ yr, although HC_3N is again somewhat over-abundant. The C_6H^- anion-to-neutral ratio is found to be quite sensitive to the effects of gas-grain interactions at this density; in the absence of accretion (Model I), $[\text{C}_6\text{H}^-]/[\text{C}_6\text{H}] = 1.3\%$ at 10^4 yr (significantly less than observed values; see Table 2). With accretion and no desorption (Model II), $[\text{C}_6\text{H}^-]/[\text{C}_6\text{H}] = 8\%$ and rises sharply as time goes on (see Figure 5). When cosmic-ray-induced desorption of atoms is accounted for (Model III), $[\text{C}_6\text{H}^-]/[\text{C}_6\text{H}]$ levels off after $\sim 10^4$ yr at about 3%, which matches well with the observations of L1544 and L1521F, but somewhat less well with the greater value of 9.3% in L1527.

Dissociative electron attachment (DEA) to the linear carbene C_6H_2 has been suggested as a potentially important route to the formation of C_6H^- in L1527 (Sakai et al. 2007). This reaction was shown to be likely to proceed rapidly in the ISM by the theoretical calculations of Herbst & Osamura (2008). In our models, C_6H_2 is included as the more stable poly-acetylene isomer, and reactions leading to the carbene(s) are neglected due to a lack of laboratory data. The observed (linear carbene) C_6H_2 abundances in TMC-1 and L1527 are reproduced if about 1-2% of the total C_6H_2 in our models is assumed to be in the form of the carbene isomer. If the poly-acetylene to carbene ratio is fixed at 1%, inclusion of the reaction

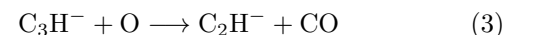


with a rate coefficient of $4.98 \times 10^{-7} (T/300)^{-0.5} \text{ cm}^3 \text{ s}^{-1}$ (Herbst & Osamura 2008), generally raises the C_6H^- abundances in our models by only a negligibly small amount.

C_6H_2 is destroyed predominantly by reacting with atomic carbon to produce $\text{C}_7\text{H} + \text{H}$. Its abundance is therefore sensitive to the gas-phase C-atom abundance. At $n_{\text{H}_2} = 10^5 \text{ cm}^{-3}$ in Model II (where C atoms are less abundant than in any of the other models), the C_6H_2 abundance can become sufficiently large (1.6×10^{-9} at 7×10^4 yr) that DEA becomes significant, contributing about 50% to the total C_6H^- formation rate. Observations of C_6H_2 in L1512 and other clouds of similar density will be required to further examine the possible significance of DEA for interstellar anion production. DEA is not expected to proceed for carbenes smaller than C_6H_2 because the reaction becomes endothermic, with an energy barrier exceeding the electron temperature in dense interstellar clouds (Herbst & Osamura 2008).

4. C_2H^-

The C_2H^- radiative electron attachment rate is calculated to be very small ($2 \times 10^{-15} (T/300)^{-0.5} \text{ cm}^3 \text{ s}^{-1}$; Herbst & Osamura 2008). As such, little C_2H^- has previously been expected in the ISM. However, the dominant production mechanism in our models is *via* the rapid reaction



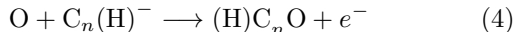
the rate of which is derived from interpolation of the $\text{C}_4\text{H}^- + \text{O}$ and $\text{C}_2\text{H}^- + \text{O}$ rates measured by Eichelberger et al. (2007) (and divided by two to account

for the 50% branching ratio adopted for the associative electron detachment channel).

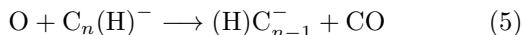
In Model III, the calculated C_2H^- fractional abundance is 6.6×10^{-14} at $t = 10^5$ yr for $n_{H_2} = 10^4$ cm^{-3} and 5.9×10^{-14} at $t = 10^4$ yr for $n_{H_2} = 10^6$ cm^{-3} . These abundances are low, but may be sufficient to permit detection with current or future radio telescopes. Agúndez et al. (2008) obtained upper limits on the C_2H^- column densities in TMC-1 and L1527 of 2.2×10^{11} and 1.8×10^{10} cm^{-2} respectively, which correspond to fractional abundance upper limits of 2.2×10^{-11} and 3.0×10^{-13} . A deeper search for C_2H^- in TMC-1 and L1527 would thus provide a useful test of our theory with regard to anion reactions with O-atoms.

5. CARBON CHAIN OXIDES

In the laboratory experiments of Eichelberger et al. (2007) on the rate of reaction of atomic oxygen with $C_n(H)^-$, a loss of ion signal was observed over time (V. Bierbaum and Y. Zhibo, private communication, 2010). This effect is attributable to associative electron detachment (AED) reactions



The raw, unpublished laboratory data are consistent with a branching ratio for AED of approximately 0.5. It must be emphasised, however, that AED products were not directly observed, and the existence of the implied carbon-chain-oxide product channels can only be definitively confirmed by additional dedicated laboratory studies. We assume the alternative product channel (with braching ratio 0.5) to result in formation of a CO molecule and a smaller anion (as described in the previous section on C_2H^-):



Model calculations were performed using an AED branching ratio of 0.5 in the reaction of oxygen with the most abundant anions in the model: C_6^- , C_7^- , C_6H^- and C_7H^- , to produce C_6O , C_7O , HC_6O and HC_7O , respectively. In addition to the new carbon-chain-oxide neutrals, their anions, cations and protonated forms were also added to the model. Radiative electron attachment rates for C_6O and C_7O were calculated assuming immediate formation of the stable anion (through vibronic transitions), following s-wave electron capture based on the method of Herbst & Osamura (2008). The degeneracies of the ground states of C_nO for n odd and even are 1 and 3 respectively, and 4 for the C_nO^- anions (based on the electronic structure calculations of Rienstra-Kiracofe et al. 2000), which leads to radiative electron attachment rates of $3.26 \times 10^{-7}(T/300)^{-0.5}$ $cm^3 s^{-1}$ for C_6O and $9.78 \times 10^{-7}(T/300)^{-0.5}$ $cm^3 s^{-1}$ for C_7O . In the absence of detailed electronic structure information for the HC_6O^- and HC_7O^- anions, an approximate radiative attachment rate coefficient of $10^{-7}(T/300)^{-0.5}$ $cm^3 s^{-1}$ has been used.

Based on the reactions and rate coefficients of the structurally similar cumulene oxide C_3O in the RATE06 database, the new carbon-chain-oxides have been assumed to undergo charge transfer reactions with H^+

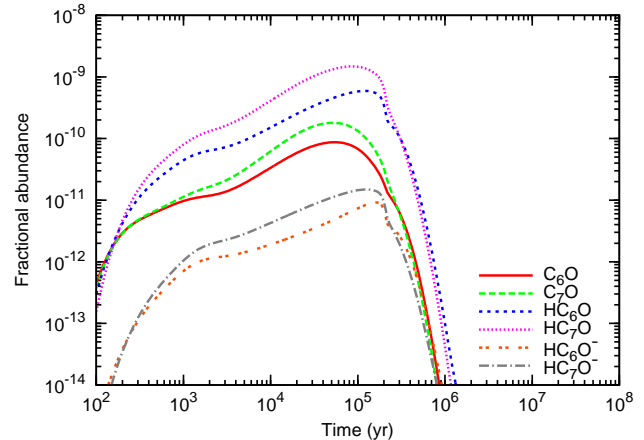


FIG. 4.— Modelled carbon-chain-oxide fractional abundances as a function of time from Model III at $n_{H_2} = 10^4$ cm^{-3} .

and C^+ , dissociative charge-transfer with He^+ and C^+ and protonation by H_3O^+ and HCO^+ . Their cations have been assumed to react with H_2 and to undergo dissociative electron recombination. For the recombination of HC_nO^+ and $H_2C_nO^+$, an H atom is assumed to be ejected, whereas for C_nO^+ , a CO molecule is assumed to be ejected. Due to the low fractional abundances of these ions ($\sim 10^{-12}$), assuming alternative recombination products (e.g. $HC_nO^+ + e^- \longrightarrow C_{(n-1)H} + CO$), has a negligible effect on the abundances of the species of interest in this study. Reactions of $(H)C_nO^-$ with H and C atoms (modelled using generic rate coefficients of 10^{-9} $cm^3 s^{-1}$), are assumed to result in associative detachment (as observed in the laboratory for hydrocarbon chain anions by Eichelberger et al. 2007); their reaction with O-atoms is assumed to result in the production of a CO_2 molecule and an anion. The $(H)C_nO^-$ anion destruction mechanisms are through photodissociation and mutual neutralisation with the most abundant cations at a rate $7.51 \times 10^{-7}(T/300)^{-0.5}$ $cm^3 s^{-1}$ (Walsh et al. 2009). Thus, although additional reactions are likely, we anticipate that the most rapid processes involving these new carbon-chain-oxide species have been – at least approximately – accounted for.

The abundances of the carbon chain oxides C_7O , HC_7O and their anions (calculated at $n_{H_2} = 10^4$ cm^{-3} using Model III), are plotted as a function of time in Figure 4. The calculated abundances of these modelled oxides and their anions are given for densities applicable to TMC-1 and L1544 in Table 3. Around the time of best agreement of the $n_{H_2} = 10^4$ cm^{-3} results with observations of TMC-1 ($\sim 10^5$ yr), the C_6O and C_7O abundances are 6.8×10^{-11} and 1.3×10^{-10} respectively. The HC_6O and HC_7O abundances are 5.8×10^{-10} and 1.5×10^{-9} respectively. These are comparable to the C_3O abundance observed in TMC-1 by Brown et al. (1985) of 1.4×10^{-10} , which suggests that large carbon chain oxides may be detectable in TMC-1 and similar carbon-chain-rich clouds. The predicted carbon-chain-oxide abundances depend on the availability of gas-phase O-atoms and are therefore significantly less in the higher-density environment of L1544 as a result of depletion of O-atoms onto dust.

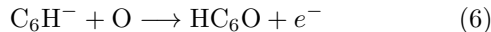
TABLE 3
MODELED FRACTIONAL ABUNDANCES OF
CARBON-CHAIN-OXIDE NEUTRALS AND
ANIONS

Species	TMC-1	L1544
C ₃ O	2.31×10^{-10}	5.77×10^{-11}
C ₆ O	6.78×10^{-11}	2.35×10^{-12}
C ₇ O	1.33×10^{-10}	1.02×10^{-12}
HC ₆ O	5.81×10^{-10}	2.58×10^{-12}
HC ₇ O	1.46×10^{-09}	2.16×10^{-12}
C ₆ O ⁻	6.20×10^{-12}	1.25×10^{-13}
C ₇ O ⁻	2.08×10^{-11}	1.16×10^{-13}
HC ₆ O ⁻	7.38×10^{-12}	2.79×10^{-14}
HC ₇ O ⁻	1.45×10^{-11}	1.25×10^{-14}

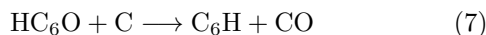
NOTE. — Fractional abundances (with respect to n_{H_2}) are from Model III, with $n_{\text{H}_2} = 10^4 \text{ cm}^{-3}$, $t = 10^5 \text{ yr}$ for TMC-1, and $n_{\text{H}_2} = 10^6 \text{ cm}^{-3}$, $t = 10^4 \text{ yr}$ for L1544.

The most important route to the smaller cumulene oxide C₃O in our model is through the dissociative recombination of H₃C₃O⁺, which is formed from the reaction of C₂H₃⁺ with CO. We do not consider the equivalent mechanisms for C₆O or C₇O synthesis (*via* C₅H₃⁺ and C₆H₃⁺, respectively), because these ions are much less abundant in the model than C₂H₃⁺, especially at early times.

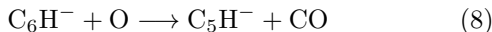
The addition of carbon-chain oxides to our models has a relatively minor impact on the abundances of other species. They act to boost the abundances of long carbon chains and anions by a few percent due to a recycling effect, for example:



followed by



whereas in previous models (*e.g.* Walsh et al. 2009), O-atom reactions resulted only in the shortening of carbon chains through CO formation:



Further dedicated laboratory studies are required in order to firmly establish the products of reactions between anions and oxygen atoms. In addition, observational searches for carbon-chain oxides and their anions will help to constrain the relevant branching ratios. The neutral (H)C_{*n*}O species (for $n = 6, 7$) have known rotational spectra and possess large dipole moments, making them suitable candidates for radio-astronomical searches.

6. TEMPORAL EVOLUTION OF THE ANION-TO-NEUTRAL RATIO

Figure 5 shows the behaviour of the C₆H⁻ anion-to-neutral ratios as a function of time at H₂ densities of 10⁴, 10⁵ and 10⁶ cm⁻³ (red, green and blue curves, respectively), for each of the three models (I-III). The anion-to-neutral ratio patterns for C₆H⁻ are representative of those for the other hydrocarbon anions in the model, and show clear variation as a function of cloud age and density. The anion-to-neutral ratio curves are distinctly different between the three models primarily as a result

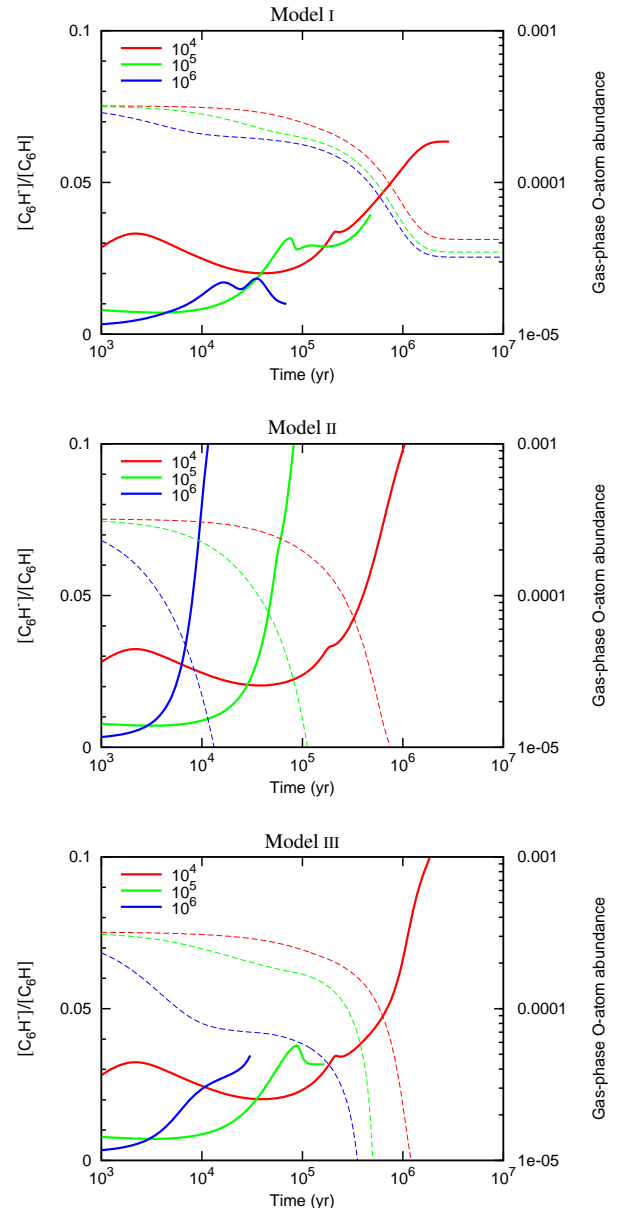


FIG. 5.— Solid lines show modelled C₆H⁻ anion-to-neutral ratios (left ordinate, linear scale) as a function of time for gas densities $n_{\text{H}_2} = 10^4 - 10^6 \text{ cm}^{-3}$ in the case of no accretion (Model I; top), freeze-out accretion (Model II; middle) and accretion + CR-desorption (Model III; bottom). Curves have been truncated when neutral C₆H fractional abundances fall below 10^{-14} . Dashed lines show the modelled gas-phase atomic oxygen fractional abundances (right ordinate, logarithmic scale).

of their dependence on the gas-phase abundances of electrons and atomic H, C and O, which themselves vary with time and density. A common trend between the three models is that in denser media, faster cation recombination rates reduce the free electron abundances during the early stages of cloud evolution, resulting in lower anion production rates. At all modelled densities, the anion-to-neutral ratios tend to increase over time as H, C and O abundances fall and electron abundances rise.

For reference, at $n_{\text{H}_2} = 10^6 \text{ cm}^{-3}$ our electron abundance as a function of time closely matches that shown

in Figure 1 of Roberts et al. (2003). In our Model II (Figure 5, middle panel), the steep rise in the anion-to-neutral ratio is mainly a consequence of the rising electron abundance that occurs during the advanced stages of freeze-out. Dashed lines in Figure 5 show the gas-phase O-atom fractional abundance, which may be used as an indicator for the level of depletion. We note that our models show qualitative agreement with the trends in the CO depletion levels (δ_{CO}) observed in TMC-1, L1512 and L1544; the CO goes from almost undepleted in TMC-1 to highly-depleted in the denser gas of L1544 (see Table 2).

Comparing Models I and II (top and middle panels of Figure 5), the effects of gas-grain interactions are clear. Gas-phase species (especially lighter, atomic species), freeze out onto the dust grains at a faster rate in denser media, which has a strong impact on the anion abundances over time: C_6H^- reacts quickly with atomic oxygen (Eichelberger et al. 2007), so the depletion of O from the gas contributes towards a steady rise in $[\text{C}_6\text{H}^-]/[\text{C}_6\text{H}]$. As the depletion of gas-phase species proceeds towards total freeze-out – indicated in the figures by the rapidly falling O-atom abundances – electron densities rise by a factor of a few. This occurs primarily as a result of the falling abundances of H_3O^+ and HCO^+ . These species have rapid recombination rates, so their loss results in elevated electron densities. Accordingly, the $[\text{C}_6\text{H}^-]/[\text{C}_6\text{H}]$ ratio rises to $\sim 50\%$ towards the end of the cloud’s lifetime (*i.e.* towards the time of complete freeze-out).

Such large anion-to-neutral ratios are incompatible with the interstellar anion observations made thus far (shown in Table 2). Given the steeply-rising nature of the $[\text{C}_6\text{H}^-]/[\text{C}_6\text{H}]$ curves in Model II and the fact that the C_6H^- abundance remains at an observable level ($\gtrsim 10^{-13}$) until relatively late times, a broad range of anion-to-neutral ratios from approximately 0-50% is predicted. However, all values observed so far have been less than 10%. It seems statistically unlikely that observations have captured only the youngest clouds on the lower parts of these curves.

Upon inclusion of cosmic-ray-induced desorption of atoms in Model III (Figure 5, bottom panel), the anion-to-neutral ratios in clouds with $n_{\text{H}_2} = 10^5 \text{ cm}^{-3}$ and $n_{\text{H}_2} = 10^6 \text{ cm}^{-3}$ obtain values of only a few percent, which are consistent with observations. Including desorption in these models keeps the electron density at a steady value of $\sim 10^{-8} n_{\text{H}_2}$ throughout the time of peak carbon-chain synthesis until well after the $\text{C} \rightarrow \text{CO}$ conversion has occurred. As a result, radiative electron attachment rates and hence anion abundances remain approximately constant (within a factor of a few) for most of the cloud’s lifetime. At $n_{\text{H}_2} = 10^4 \text{ cm}^{-3}$, the results match observations at ‘early time’ ($\sim 10^5 \text{ yr}$), but towards later times, $[\text{C}_6\text{H}^-]/[\text{C}_6\text{H}]$ continues to rise (due to rising electron densities), and levels off at just over 10%. This result implies that anion-to-neutral ratios greater than presently observed may be detectable in quiescent clouds significantly older than TMC-1. The decline of carbon-chain abundances at late times will make such observations challenging, however.

7. DISCUSSION

The C_6H^- anion-to-neutral ratio observed in L1527 (9.3%) is significantly larger than in the other sources with similar densities (see Table 2). Accordingly, Model III gives a poorer agreement with L1527 than L1544 and L1521F. This discrepancy might be related to the presence of the low-mass protostar IRAS 04368+2557 at the center of L1527, heating from which is not accounted for by our model. Fits to the sub-mm SED have shown that the dust surrounding IRAS 04368+2557 has a temperature of 22-35 K. The large abundances of carbon-chain-bearing molecules (including C_nH , C_nH^- , HC_nN and CH_3CCH) observed by Sakai et al. (2008) have been interpreted as arising in the warm protostellar envelope as a result of ‘warm carbon-chain chemistry’. It has been theorized that in this region, methane ice sublimates from the dust grain surfaces and participates in a gas-phase chemistry which results in the production of large abundances of carbon-chain-bearing species.

Harada & Herbst (2008) modelled the gas-phase chemistry of L1527 using a similar approach to our Model I (with $n_{\text{H}_2} = 10^6 \text{ cm}^{-3}$), but with initial abundances appropriate for a protostellar envelope at 30 K. Volatile molecular ices (including CO and CH_4) were theorized to have been formed on the dust, then released into the gas phase during protostellar warm-up. The large initial gas-phase methane abundance used by Harada & Herbst (2008) results in greatly-accelerated synthesis of carbon-chain-bearing species as a result of ion-molecule chemistry (see *e.g.* Brown & Charnley 1991; Hassel et al. 2008), which explains why their modelled polyene and cyanopolyene abundances (Harada & Herbst 2008, Figure 5) are able to match observations after only a few thousand years. Our Models II and III, on the other hand, give a satisfactory agreement with this source after $\sim 10^4 \text{ yr}$, and show that warm carbon-chain chemistry is not necessarily required to explain the large carbon chain abundances in this source. Instead, the depletion of oxygen atoms onto dust may be sufficient to permit an efficient carbon chain chemistry to develop. The presence of abundant hydrocarbon anions is also likely to boost the abundances of carbon-chain-bearing species (see Walsh et al. 2009). However, warm-up chemistry may explain the elevated L1527 anion-to-neutral ratio if it can produce greater electron densities or reduced H and O-atom abundances; to test these ideas would require a more detailed chemical model. Indeed, Harada & Herbst (2008) calculated a C_6H^- anion-to-neutral ratio of about 50% in L1527 (five times greater than observed), which is likely to be at least partly a result of their low initial H, C and O-atom abundances, which are several orders of magnitude less than ours.

Agreement of our model with observations at $t \sim 10^4 \text{ yr}$ is in apparent contradiction with the age of L1527, which is likely to be $\gtrsim 10^5 \text{ yr}$ based on the estimated length of the pre-stellar core phase ($\sim 10^5 \text{ yr}$; Kirk et al. 2005). However, the gas in the protostellar envelope has undergone collapse from lower density to arrive at the present value of $n_{\text{H}_2} = 10^6 \text{ cm}^{-3}$. Given the density-dependence of the timescale for formation of peak carbon chain abundances (see Figures 1-3), our derived time-of-best-agreement cannot be treated as a reliable age indicator.

The adopted initial abundances for our models (Table 1) assume the cloud evolves from a neutral state at $t = 0$.

This is contrary to Walsh et al. (2009) who assumed all the C and S atoms to be initially ionized. As can be seen by comparing the results of our $n_{\text{H}_2} = 10^4 \text{ cm}^{-3}$ model with theirs, the choice of initial ionisation conditions has a profound impact on the neutral and anionic polyne abundances at very early times ($t \lesssim 500 \text{ yr}$). The large abundance of free electrons in the ‘initially-ionized’ model results in rapid anion production. Consequently, given the propensity of hydrocarbon anions to stimulate synthesis of enhanced polyne and polyacetylene abundances *via* anion-neutral reactions, the carbon-chain-bearing species can reach abundances orders of magnitude greater than in our ‘initially-neutral’ models. The density-dependence of the chemical timescales (see Section 3) determines whether this ‘very early-time’ peak in carbon chain abundances has any lasting impact on the abundances of the species of interest.

For instance, at $n_{\text{H}_2} = 10^4 \text{ cm}^{-3}$, by the time of best fit with observations ($t \sim 10^5 \text{ yr}$), the abundances in the initially-neutral and initially-ionized models have converged so as to be practically indistinguishable. The same can also be said for the models at $n_{\text{H}_2} = 10^5 \text{ cm}^{-3}$. However, towards higher densities ($n \gtrsim 10^6 \text{ cm}^{-3}$), convergence does not occur sufficiently quickly, and the elevated carbon chain abundances persist through until the time of freeze-out. These effects are more pronounced for longer carbon chains, and as a result, the C_6H abundance is about a factor of two greater for $n_{\text{H}_2} = 10^6 \text{ cm}^{-3}$ at around the time of best fit with observations ($t \sim 10^4 \text{ yr}$), when carbon is initially ionized. Anion-to-neutral ratios are also greater by a factor of about 0.5. Although still in good agreement with observations, it is deemed that models with C (and S) initially ionized are less representative of the conditions present in such dense clouds, which are generally found in regions of high extinction where ionizing UV photons cannot penetrate and the gas is therefore neutral.

Regarding the possible use of anions as chemical probes, the reaction rates of C_6H^- with O and H atoms were measured in the laboratory by Eichelberger et al. (2007) as 5.4×10^{-10} and $5.0 \times 10^{-10} \text{ cm}^3 \text{ s}^{-1}$, respectively. Because of this similarity, the dominant C_6H^- destruction mechanisms can be considered to be by reaction with H atoms for gas-phase $[\text{O}]/[\text{H}] < 1$ and by reaction with O-atoms for $[\text{O}]/[\text{H}] > 1$. Although we use a slightly larger rate for reactions of C_6H^- with C-atoms ($1.0 \times 10^{-9} \text{ cm}^3 \text{ s}^{-1}$), the C-atom abundances remain sufficiently low in our models that this reaction is never a competitive cause of C_6H^- destruction. The N-atom destruction reactions are also a couple of orders of magnitude less rapid. At a density $n_{\text{H}_2} = 10^4 \text{ cm}^{-3}$, H is more abundant than O by a factor of at least 2.5 for all times in each of our models. However, at higher densities ($n_{\text{H}_2} \gtrsim 10^5 \text{ cm}^{-3}$) – as a consequence of the more rapid gas-phase chemistry and H_2 formation on dust – H becomes up to 2 orders of magnitude less abundant than O at early times. In these circumstances, at around the times of best agreement of the models with observations, the anion abundances are closely dependent on the O-atom abundances. Anion abundances are also sensitive to the number density of free electrons. Therefore, if the electron abundance is known, anion-to-neutral ratios may be used as a probe of the gas-phase oxygen abun-

dance in dense interstellar clouds.

The absolute and relative carbon chain and anion abundances in our models are dependent on the gas accretion rates, which scale with the total dust grain surface area and the sticking coefficients, both of which are subject to uncertainty. To address this, we have run models employing a factor of four range in dust surface area (by taking $X'_G = 2X_G$ and $X'_G = X_G/2$), and find that although the modelled abundances and times of best agreement with observations change slightly (greater differences occurring in the higher-density models), the overall results of our study are unaffected. Increased accretion rates ($X'_G = 2X_G$) lead to a stronger, earlier freeze-out peak in the polyne and anion abundances, combined with a steeper rise in the electron abundances and anion-to-neutral ratios at late times. Reduced accretion rates ($X'_G = X_G/2$), on the other hand, result in significantly greater late-time abundances, allowing complex molecules to exist in the gas for almost twice as long. Examination of the effects of species-dependent differential accretion rates, further to what may be inferred from our treatment of atomic desorption in Model III, is beyond the scope of the present study.

8. SUMMARY

Similar to previous models for anions in TMC-1 (Millar et al. 2007; Walsh et al. 2009), for a density of $n_{\text{H}_2} = 10^4 \text{ cm}^{-3}$ we obtain good agreement between modelled and observed anion-to-neutral ratios and absolute polyne abundances at times $\sim 10^5 \text{ yr}$. Similarly good agreement is found for the quiescent cloud Lupus 1A. This result is independent of the inclusion of gas-grain interactions, which are negligible at this time and for this relatively low gas density. Models give a poor fit with observations at later times due to their falling cyanopolyne abundances, although the freeze-out of atomic oxygen does permit the polyynes to remain abundant up to $\sim 10^6 \text{ yr}$.

The chemical timescale for the formation of abundant carbon-chain-bearing species (including the polyynes, cyanopolyynes and hydrocarbon anions) is inversely dependent on the cloud density. Thus, for clouds of moderate density ($n_{\text{H}_2} = 10^5 \text{ cm}^{-3}$), such as L1512 and L1251A, the best fits between modelled and observed abundances of carbon-chain-bearing species occur at earlier times ($\sim 7 \times 10^4 \text{ yr}$). At this higher density, Models I (no accretion) and III (accretion + CR-desorption) match the observations better than Model II (accretion with no desorption).

At densities $n_{\text{H}_2} = 10^6 \text{ cm}^{-3}$, the best fit with observations of L1544, L1521F and L1527 is for Model III, at $t \sim 10^4 \text{ yr}$. We find that by accounting for gas-grain interactions (in particular, the freeze-out of atomic oxygen), the large observed abundances of carbon-chain-bearing species in these environments can be reproduced. However, a sufficient number of small O-bearing ions are required to remain in the gas-phase to maintain a steady electron abundance and therefore keep the radiative electron attachment rates down, in order to reproduce the relatively low observed anion-to-neutral ratios (on the order of a few percent) in L1544 and L1521F. Without atomic desorption, rising electron abundances around the time of freeze-out result in excessively large anion-to-neutral ratios.

In summary, the gas-grain interaction, through its influence on the chemistry (in particular, the O and H-atom abundances and the electron density), is found to have profound effects on the abundances of carbon-chain-bearing species and their anions in dense interstellar clouds with $n_{\text{H}_2} \gtrsim 10^5$. Due to their destructive reactions with atomic oxygen, neutral and anionic polyynes are predicted to be most abundant in oxygen-depleted environments. In addition, O-atom + anion reactions are found to have the potential to produce as-yet unobserved interstellar species including carbon-chain oxides and C_2H^- .

The sensitivity of the interstellar C_6H^- anion-to-

neutral ratio to the gas-phase O, H and e^- abundances could allow anions to be used as a probe of these fundamental chemical species.

We acknowledge Dr. Catherine Walsh for assistance in development of the anion chemical network and Prof. Veronica Bierbaum and Dr. Zhibo Yang for sharing their laboratory data pertaining to reactions between oxygen atoms and anions. This research was supported NASA's Exobiology and Origins of Solar Systems programs and by the NASA Astrobiology Institute through the Goddard Center for Astrobiology.

REFERENCES

- Agúndez, M., Fonfría, J. P., Cernicharo, J., Pardo, J. R., Guélin, M. 2008, *A&A*, 479, 493
- Agúndez, M., Cernicharo, J., Guélin, M., et al. 2010, *A&A*, 517, L2
- Brown, R. D., Godfrey, P. D., Cragg, D. M., et al. 1985, *ApJ*, 297, 302
- Brown, P. D., Charnley, S. B. 1991, *MNRAS*, 249, 69
- Brown, P. D., Charnley, S. B. 1990, *MNRAS*, 244, 432
- Brünken, S., Gupta, H., Gottlieb, C. A., McCarthy, M. C., Thaddeus, P. 2007, 664, L43
- Buckle, J. V., Rodgers, S. D., Wirstrom, E. S. et al. 2006, *Faraday Discuss.*, 133, 63
- Caselli, P., Walmsley, M., Zucconi, A., et al. 2002, *ApJ*, 565, 331
- Cernicharo, J., Guélin, M. 1987, *A&A*, 176, 299
- Cernicharo, J., Guélin, M., Agúndez, M., Kawaguchi, K., McCarthy, M., Thaddeus, P. 2007, *A&A*, 467, 37
- Charnley, S. B. 1997, *MNRAS*, 291, 455
- Charnley, S. B., Rodgers, S. D., Ehrenfreund, P. 2001, *A&A* 378, 1024
- Cordiner, M. A., Millar, T. J., Walsh, C. et al. 2008, *IAUS*, 251, 157
- Cordiner, M. A., Millar, T. J. 2009, *ApJ*, 697, 68
- Cordiner, M. A., Charnley, S. B., Buckle, J. V., Walsh, C., Millar, T. J. 2011, *ApJ*, 730, L18
- Crapsi, A., Caselli, P., Walmsley, C. M., et al. 2004, *A&A*, 420, 957
- Crapsi, A., Caselli, P., Walmsley, C. M., et al. 2005, *ApJ*, 619, 379
- Eichelberger, B., Snow, T. P., Barckholtz, C., Bierbaum, V. M. 2007, *ApJ*, 667, 1283
- Flower, D. R., Pineau Des Forêts, G., Walmsley, C. M. 2007, *A&A*, 474, 923
- Flower, D. R., Pineau Des Forêts, G.; Walmsley, C. M. 2005, *A&A*, 436, 933
- Gupta, H., Gottlieb, C. A., McCarthy, M. C., Thaddeus, P. 2009, *ApJ*, 691, 1494
- Hasegawa, T. I., Herbst, E. 1993, *MNRAS*, 261, 83
- Harada, N., Herbst, E. 2008, *ApJ*, 685, 272
- Hassel, G. E., Herbst, E., Garrod, R. T. 2008, 681, 1385
- Herbst, E., Leung, C. M. 1989, *ApJSS*, 69, 271
- Herbst, E., Osamura, Y. 2008, *ApJ*, 679, 1670
- Hirahara, Y., Suzuki, H., Yamamoto, S. 1992, *ApJ*, 394, 539
- Jørgensen, J. K., Schöier, F. L., van Dishoeck, E. F. 2004, *A&A*, 416, 603
- Jørgensen, J. K., Schöier, F. L., van Dishoeck, E. F. 2002, *A&A*, 389, 908
- Kirk, J. M., Ward-Thompson, D., André, P. 2005, *MNRAS*, 360, 1506
- Leger, A., Jura, M., Omont, A. 1985, *A&A*, 144, 147
- Lee, J., Evans, N. J., Shirley, Y. L., Tatematsu, K. 2003, *ApJ*, 583, 789
- Lee, J., Lee, H. G., Shinn, J., et al. 2010, *ApJ*, 709, 74
- Lepp, S., Dalgarno, A. 1988, *ApJ*, 324, 553
- McCarthy, M. C., Gottlieb, C. A., Gupta, H. C., Thaddeus, P. 2006, *ApJL*, 652, L141
- Millar, T. J., Walsh, C., Cordiner, M. A., Ní Chuimín, R., Herbst, E. 2007, *ApJL*, 662, L87
- Öberg, K. I., Boogert, A. C. A., Pontoppidan, K. M. et al. 2011, *ApJ*, 740, 109
- Ohishi, M., Irvine, W. A., Kaifu, N. 1992, *IAUS*, 150, 1710
- Peeters, E. 2011, *EAS Publications Series*, 46, 13
- Remijan, A. J., Hollis, J. M., Lovas, F. J., et al. 2007, *ApJL*, 664, L47
- Rienstra-Kiracofe, J. C., Ellison, G. B., Hoffman, B. C., Schaefer, H. F. III. 2000, *J. Phys. Chem. A*, 104, 2273
- Roberts, H., Herbst, E., Millar, T. J. 2003, *ApJ*, 591, L41
- Smith, I. W. M., Herbst, E., Chang, Q. 2004, *MNRAS*, 350, 323
- Sakai, N., Sakai, T., Osamura, Y., Yamamoto, S. 2007, *ApJ*, 667, L65
- Sakai, N., Sakai, T., Hirota, T., Yamamoto, S. 2008, *ApJ*, 672, 371
- Sakai, N., Shiino, T., Hirota, T., Sakai, T., Yamamoto, S. 2010, *ApJ*, 718, L49
- Suzuki, H., Yamamoto, S., Ohishi, M. et al. 1992, *ApJ*, 392, 551
- Thaddeus, P., Gottlieb, C. A., Gupta, H. et al. 2008, *ApJ*, 677, 1132
- Turner, B. E. 1991, *ApJ*, 376, 573
- Umebayashi, T., Takenori, N. 1990, *MNRAS*, 243, 103
- Wakelam, V., Herbst, E. 2008, *ApJ*, 680, 371
- Walsh, C., Harada, N., Herbst, E., Millar, T. J. 2009, *ApJ*, 700, 725
- Woodall, J., Agúndez, M., Markwick-Kemper, A. J., Millar, T. J. 2007, *A&A*, 466, 1197